Earth and Planetary Science Letters 435 (2016) 36–44

Contents lists available at ScienceDirect

Earth and Planetary Science Letters

www.elsevier.com/locate/epsl

Thermal recalcitrance of the organic D-rich component of ordinary chondrites

L. Remusat [a,*], L. Piani [a,b], S. Bernard [a]

[a] Institut de Minéralogie, de Physique des Matériaux, et de Cosmochimie (IMPMC), UMR CNRS 7590 – Sorbonne Universités – UPMC – IRD – Muséum National d'Histoire Naturelle, 57 rue Cuvier, Case 52, 75231 Paris Cedex 5, France
[b] Department of Natural History Sciences, Hokkaido University, Sapporo 060-0810, Japan

ARTICLE INFO

Article history:
Received 26 June 2015
Received in revised form 25 November 2015
Accepted 5 December 2015
Available online xxxx
Editor: B. Marty

Keywords:
insoluble organic matter
chondrite
parent body processes
NanoSIMS
hydrogen and nitrogen isotopes
solar system

ABSTRACT

Carbonaceous and ordinary chondrites (CCs and OCs) contain insoluble organic matter (IOM) with large D-excess compared to other objects in the solar system. The higher the temperature experienced by CCs, the lower the D/H ratio of their IOM. It seems to be the opposite for OCs. Here, we report NanoSIMS H- (and N-) isotopic imaging of IOM of three OCs that experienced thermal metamorphism in the sequence Semarkona, Bishunpur and GRO 95502. In addition, we performed flash heating experiments on the IOM of GRO 95502 at 600 °C and characterized the residues using NanoSIMS, Raman and XANES spectroscopy. The present study shows that, in contrast to IOM of CI, CM and CR, IOM of OCs exhibits very few D-rich (or ^{15}N-rich) hotspots. Furthermore, although the evolution of the molecular structure of OC and CC IOM is similar upon heating, their D/H ratios do not follow the same trend: the D/H of OC IOM drastically increases while the D/H of CC IOM decreases. In contrast to CC IOM, the D-rich component of which does not survive at high temperatures, the present results highlight the thermal recalcitrance of the D-rich component of OC IOM. This suggests that CCs and OCs did not accrete the same organic material, thereby challenging the hypothesis of a common precursor on chondritic parent bodies. The present results support the hypothesis that OC IOM contains an organic component that could originate from the interstellar medium.

1. Introduction

Chondrites are often considered to be the witnesses of solar system formation (Weisberg et al., 2006). Their components are believed to have formed during the collapse of the parent molecular cloud and solar nebula evolution. They are consequently the targets for many studies aiming to understand the processes of formation of the constituents of planetesimals and planets. The origin of volatile reservoirs in the early solar system is the subject of intense debate, with implications for the origin of water and life on Earth. In this respect, carbonaceous chondrites (CCs) have received most of the attention because they are the most organic- and water-rich chondrites (CCs may contain up to a few weight percent of carbon). Two types of organic matter are usually distinguished (Remusat, 2015): the organic matter that is soluble in water and organic solvents, and the insoluble organic matter (IOM). The IOM constitutes the major part of the total organic material and is generally studied after isolation from the minerals by acid treatments using HF-HCl (Robert and Epstein, 1982) or CsF-HCl (Alexander et al., 2007).

The molecular, structural and chemical composition of CC IOM has been extensively documented (Remusat, 2015 and references herein). It corresponds to a macromolecule made of small aromatic units linked by short aliphatic chains that contains hetero-elements (N, S, O) (Hayatsu et al., 1980; Remusat et al., 2005; Cody and Alexander, 2005; Orthous-Daunay et al., 2010) and organic radicals (Binet et al., 2002, 2004). Type 1 and 2 CC IOM is enriched in heavy isotopes of H and N relative to terrestrial organic matter, with the exception of some CMs having near-atmospheric IOM N isotopic compositions (Robert and Epstein, 1982; Yang and Epstein, 1983; Alexander et al., 2007, 2010), and exhibits micron-sized hotspots enriched in D and ^{15}N (Busemann et al., 2006; Nakamura-Messenger et al., 2006; Remusat et al., 2009). These hotspots have been interpreted as remnants of interstellar organic compounds (Busemann et al., 2006; Nakamura-Messenger et al., 2006) or evidence of an early irradiation of the solar system (Remusat et al., 2009). Of note, at least for Murchison (CM chondrite), these hotspots disappear when the IOM is submitted to thermal treatment at 600 °C under He atmosphere (Remusat et al., 2009).

* Corresponding author.
E-mail address: remusat@mnhn.fr (L. Remusat).

http://dx.doi.org/10.1016/j.epsl.2015.12.009
0012-821X/

Despite the abundance of available samples, much less is known about organic matter in ordinary chondrites (OCs). In contrast to most CCs, which experienced aqueous alteration on parent bodies, most OCs experienced thermal metamorphism that may have led to the complete degradation of organics (Yang and Epstein, 1983; Alexander et al., 2010). Although the two falls Semarkona (LL3.0) and Bishunpur (LL3.15) exhibit some signs of secondary hydrous alteration (i.e. processes on the parent body; Alexander et al., 1989; Sears et al., 1995). Raman spectroscopy investigations on IOM have shown that Semarkona is, by far, the most pristine unequilibrated ordinary chondrite (UOC). IOM experienced a metamorphic temperature peak well below 250 °C (Quirico et al., 2003; Busemann et al., 2007); this temperature is consistent with estimates from mineral assemblage ($T < 260$ °C – Alexander et al., 1989) and sulfide thermometry (230 °C – Zanda et al., 1995). The IOM of OCs is generally richer in D than that of CCs and exhibits anticorrelated D/H and H/C ratios, in contrast to CC IOM (Alexander et al., 2007, 2010). No D- or ^{15}N-rich hotspot has ever been reported in OC IOM, as recently illustrated by NanoSIMS images of the IOM of the Krymka meteorite (LL3.2) showing no heterogeneities in D/H (Alexander et al., 2010).

The present study reports NanoSIMS H- and N- isotopic imaging of IOM of three UOCs that experienced different thermal metamorphism: Semarkona (LL3.0), Bishunpur (LL3.15) and Grosvenor Mountains (GRO) 95502 (L3.2). In addition, we document the molecular signature and structural properties of the IOM of GRO 95502 before and after flash heating experiments. The results highlight the thermal recalcitrance of the D-rich component of OC IOM and suggest that the original precursors of CC and OC organic matter were different.

2. Experimental

2.1. Samples

IOM has been isolated from three UOCs of increasing metamorphic grades: Semarkona (LL3.0), Bishunpur (LL3.15), and GRO 95502 (L3.2). Semarkona and Bishunpur IOM was prepared by Yang and Epstein (1983) by classical HF/HCl dissolution. This IOM has been stored since then at room temperature, in a glass vial sealed by a Teflon cap and protected from the sunlight. Fifty milligrams of GRO 95502 IOM (hereafter called GRO IOM) were recently isolated from 20 g of meteorite using a similar protocol (Piani et al., 2012a). An aliquot of GRO IOM was subjected to flash pyrolysis at 600 °C under a He atmosphere. The (organic) residue was recovered and is hereafter called GROpyr. Orgueil IOM, prepared by Remusat et al. (2005), was used as a reference material.

Aliquots of these IOM samples were pressed into cleaned indium foil and gold coated (20 nm thick) to improve charge compensation during NanoSIMS imaging. Portions of GRO IOM and GROpyr samples were also finely powdered in an agate mortar and deposited on Si_3N_4 windows for Raman and XANES (X-ray absorption near edge structure) investigations.

2.2. NanoSIMS settings

Isotopic images were acquired using the Cameca NanoSIMS 50 installed at the National Museum of Natural History in Paris, France. A 16 keV primary Cs^+ beam was used to collect the secondary ions H^- and D^- during a first run (to obtain δD images), and $^{16}O^-$, $^{12}C_2^-$, $^{12}C^{14}N^-$, $^{12}C^{15}N^-$ and $^{32}S^-$ during a second run (for N/C and δ^{15}N images). The use of the ion ratio $^{12}C^{14}N^-/^{12}C_2^-$ reduces topographic effects on the N/C measurements (Thomen et al., 2014; Alleon et al., 2015). The primary beam was set to 8 pA for H isotope and to 3 pA for N isotope measurements, leading to spatial resolutions of about 300 and 150 nm, respectively. We collected 256×256 pixel images covering 20×20 µm^2 with a raster speed of 2 ms/pix. Prior to each analysis, a 25×25 µm^2 presputtering was applied using a 600 pA primary current for 6 min (corresponding to a Cs^+ fluence of 2.2×10^{17} at cm^{-2}) in order to remove the gold coat, clean the surface, and reach the sputtering steady state (Thomen et al., 2014). We used Hamamatsu discrete dynode electron multipliers with a dead time of 44 ns in multicollection mode. For H isotopes, the mass spectrometer was set to a mass resolving power of 4000, and to 8000 for N isotopes to resolve isobaric interferences, such as $^{12}C^{14}N^-$ from $^{12}C_2H_2^-$ and $^{32}S^-$ from $^{16}O_2^-$. The vacuum in the analysis chamber never exceeded $5 \cdot 10^{10}$ Torr.

The collected NanoSIMS data were then processed with the L'Image software developed by Larry Nittler, Carnegie Institution in Washington DC, USA. Each image being a stack of several frames, the first step consists of aligning each frame using a correlation algorithm and applying the same shift in X and Y to all the pixels of a single frame. Then, ratio images can be generated. Each ratio is corrected using a calibration line (see supplementary material), determined by measuring four known reference samples (which in the meantime allow checking the instrument stability): a terrestrial Type 3 kerogen, a charcoal and the IOM of Orgueil and GRO 95502 (previously measured by gas source mass spectrometry by Alexander et al., 2007). Each calibration line is calculated using a linear regression and the R program was used to determine uncertainties associated with the calibration (Table S1). All the uncertainties reported in this study are one standard deviation; we propagated (using quadratic sum) counting statistics uncertainties on each regions of interest (ROI) and uncertainties arising from the calibration lines, reflecting the external precision of our measurements (e.g., the standard deviation for independent measurements repeated several times on the same sample).

Isotopic ratios are expressed in delta units, following the relation: $\delta(‰) = (R_{sple}/R_{std} - 1) \times 1000$, with R_{sple} being the sample isotopic ratio and R_{std} a reference ratio, such as Standard Mean Ocean Water (SMOW: $D/H = 155.76 \times 10^{-6}$) for H isotopes and air for N isotopes ($^{15}N/^{14}N = 3.67 \times 10^{-3}$). Isotopic anomalies in D (or in ^{15}N) are defined as ROIs consisting of at least 50 pixels (0.3 µm^2) meeting individually the requirement $|(D/H)_{pixel} - (D/H)_{average}|/\sigma > 2$ (or $|(^{15}N/^{14}N)_{pixel} - (^{15}N/^{14}N)_{average}|/\sigma > 2$), where $(D/H)_{pixel}$ (or $(^{15}N/^{14}N)_{pixel}$) is the isotopic ratio of the pixel, $(D/H)_{average}$ (or $(^{15}N/^{14}N)_{average}$) the average ratio of the image and σ the statistical error for each pixel (Table S2). Anomalies can be significantly positive or negative, reflecting enrichment or depletion in D (or ^{15}N) compared to the average of the image, respectively. The heterogeneity in the D/H ratio can be investigated using pixel histograms showing the distributions of δD (or δ^{15}N) values of individual pixels within each image. The occurrence of positive micron-scale anomalies can be noticed on these histograms. They result in tails on the right side of histograms but do not affect the full width at half maximum (FWHM). Of note, some of these anomalies may correspond to presolar grains (e.g. Floss and Stadermann, 2009). Data are reported in the supplementary material (Tables S2 and S3).

2.3. Raman and STXM/XANES characterization

Raman data were collected on powdered samples using the Renishaw INVIA microspectrometer operating at IMPMC following the procedure described in Bernard et al. (2008). Twenty spectra were collected on each IOM to capture their homogeneous or heterogeneous nature. Spectra were measured from 500 to 3500 cm^{-1} at constant room temperature using the 514.5 nm wavelength of a 50 mW Modulaser Argon laser (green laser) focused on the sample through a Leica DMLM microscope with a long working distance

50X objective (NA = 0.55). This configuration yields a planar resolution of ~1 μm for a laser power delivered at the sample surface set at around 250 μW to prevent irreversible thermal damage due to laser-induced heating (Beyssac et al., 2003). A grating with 1800 lines/mm disperses light and the signal was analyzed with a RENCAM CCD detector. Measurements are performed with a circularly polarized laser using a 1/4 wavelength plate placed before the microscope in order to limit polarization effects.

XANES data were collected using the STXM (scanning transmission X-ray microscope) located on beamline 5.3.2.2 (STXM Polymer beamline – Kilcoyne et al., 2003) at the Advanced Light Source (ALS). This beamline uses soft X-rays (250–600 eV) generated via a bending magnet while the electron current in the storage ring is held constant in top-off mode at 500 mA at a storage ring energy of 1.9 GeV. The microscope chamber is evacuated to 100 mTorr after sample insertion and back-filled with He. Energy calibration is accomplished using the well-resolved 3p Rydberg peak at 294.96 eV of gaseous CO_2 for the C K-edge. Alignment of images of stacks and extraction of XANES spectra were done using the aXis2000 software (ver2.1n) while normalization to the carbon quantity was done using the Athena software package (Ravel and Newville, 2005). The C-XANES spectra shown in the present study are for homogeneous organic-rich areas of several hundreds of nanometers. Although radiation damage per unit of analytical information was shown to be typically 100–1000 times lower in STXM-based XANES spectroscopy than in TEM-based EELS (Hitchcock et al., 2008), the C-XANES data shown here were collected following the procedures for X-ray microscopy studies of radiation sensitive samples recommended by Wang et al. (2009). Extensive databases of reference XANES spectra (measured on hundreds of C-containing compounds at the C K-edge, sometimes supported by theoretical calculations using multiple scattering approaches) are available (Solomon et al., 2009).

3. Results

3.1. NanoSIMS imaging of H isotopes

The spatial distributions of hydrogen isotopes in the OC IOM are remarkably different from that of the Orgueil IOM (Remusat et al., 2009). Semarkona and Bishunpur IOM exhibit different isotopic compositions depending on the measured area (Fig. 1). Despite their D-rich nature, the IOM of OCs exhibits fewer D anomalies than does Orgueil IOM (Busemann et al., 2006; Nakamura-Messenger et al., 2006; Remusat et al., 2009). In addition, the intensities and sizes of isotopic anomalies in OC IOM differ from those in Orgueil and other CC IOM (Fig. 2 and Table S2). Orgueil IOM exhibits numerous micron-scale D anomalies (25 over 800 μm^2, with 2000‰ < δD < 4000‰) while the average δD value is indistinguishable from one region to another. In contrast, only two micron-scale D anomalies are detected in Semarkona IOM (one positive with δD = 5000‰ and one negative with δD = 300‰) while entire regions may display significant D-enrichments (δD = 5000‰ for instance over area 2 in Fig. 1) compared to adjacent ones (δD = 2000‰ over area 1 in Fig. 1). Bishunpur IOM displays large regions with δD values ranging from 800‰ to 2700‰ and exhibits five positive (up to δD = 4000‰) and three negative (around δD = 200‰) micron-scale anomalies over 1200 μm^2. Despite three positive (5500‰ < δD < 6300‰) and four negative (1200‰ < δD < 1500‰) anomalies, the GRO IOM exhibits a quite homogeneous D/H ratio (considering about 600 μm^2 analyzed in this study), consistent with previous measurements (Piani et al., 2012a, 2015). The flash pyrolysis at 600 °C of this IOM induces a D-enrichment by a factor of 2.5 (δD = 9000‰) and seems to homogenize the D/H ratio: no significant isotopic anomalous regions

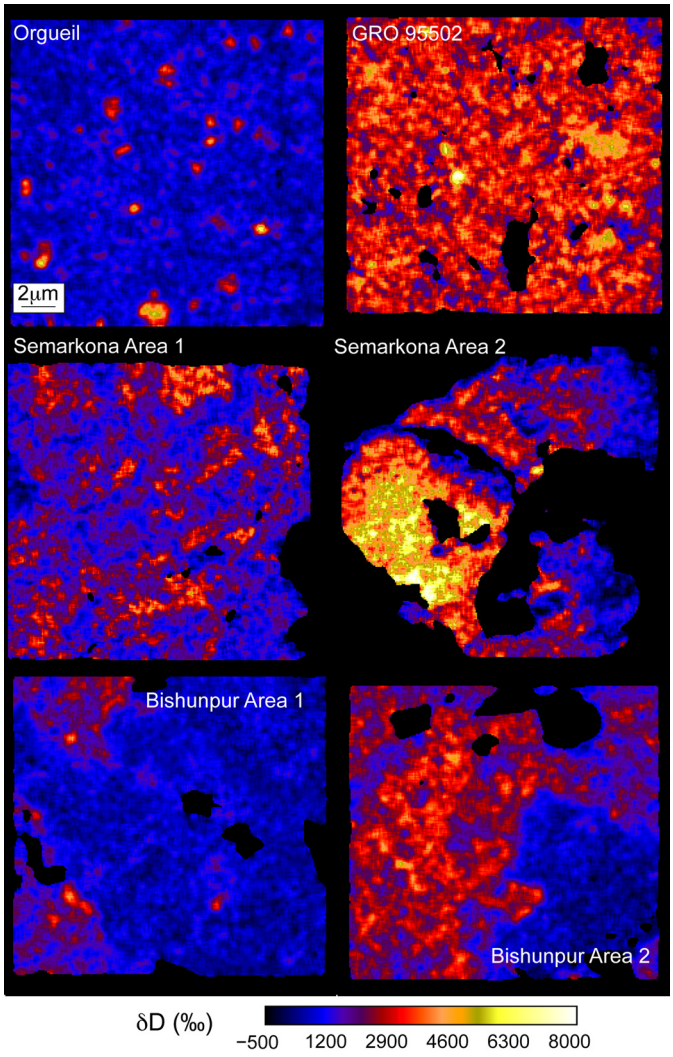

Fig. 1. NanoSIMS δD images of the IOM of Orgueil, GRO 95502, Semarkona and Bishunpur. All the images have the same size; the color scale represents corrected δD values. To illustrate the large-scale variations observed in Semarkona and Bishunpur IOM, two different areas are displayed. (Colored version of this figure is available in the web version of this article.)

can be distinguished within GROpyr over 2170 μm^2 surface area analyzed (Fig. 3, Fig. S3 and Table S2).

The histograms of the δD values of individual pixels in the IOM of the OCs are different from the histograms usually observed for Type 1 and 2 CCs (Fig. 4). For Orgueil, the δD histogram is rather narrow, with asymmetry arising from the occurrence of numerous D-rich hotspots on the right side (high values). The tight width of Orgueil IOM histogram indicates that most of the IOM has a homogeneous isotopic ratio representing the bulk value of this IOM, the hot spots only representing some material in the tail of the histogram for the larger values. The contribution of the D-rich hotspot pixels to the total images of Orgueil IOM has previously been shown to be small (Remusat et al., 2009). For the Semarkona and Bishunpur IOM (Fig. 4), the δD histograms are broader and appear bimodal (see area 2 in both IOM in Fig. 4). These histograms are fully consistent with the large differences in the average image δD of Semarkona and Bishunpur IOM (Fig. 2) and constitute suitable tools to assess micron-scale isotopic distributions in IOM. Interestingly, the D-poor component in Bishunpur area 2 has the same isotopic signature as the material in Bishunpur area 1. In contrast, the δD histogram of the GRO IOM (Fig. 4) indicates a ho-

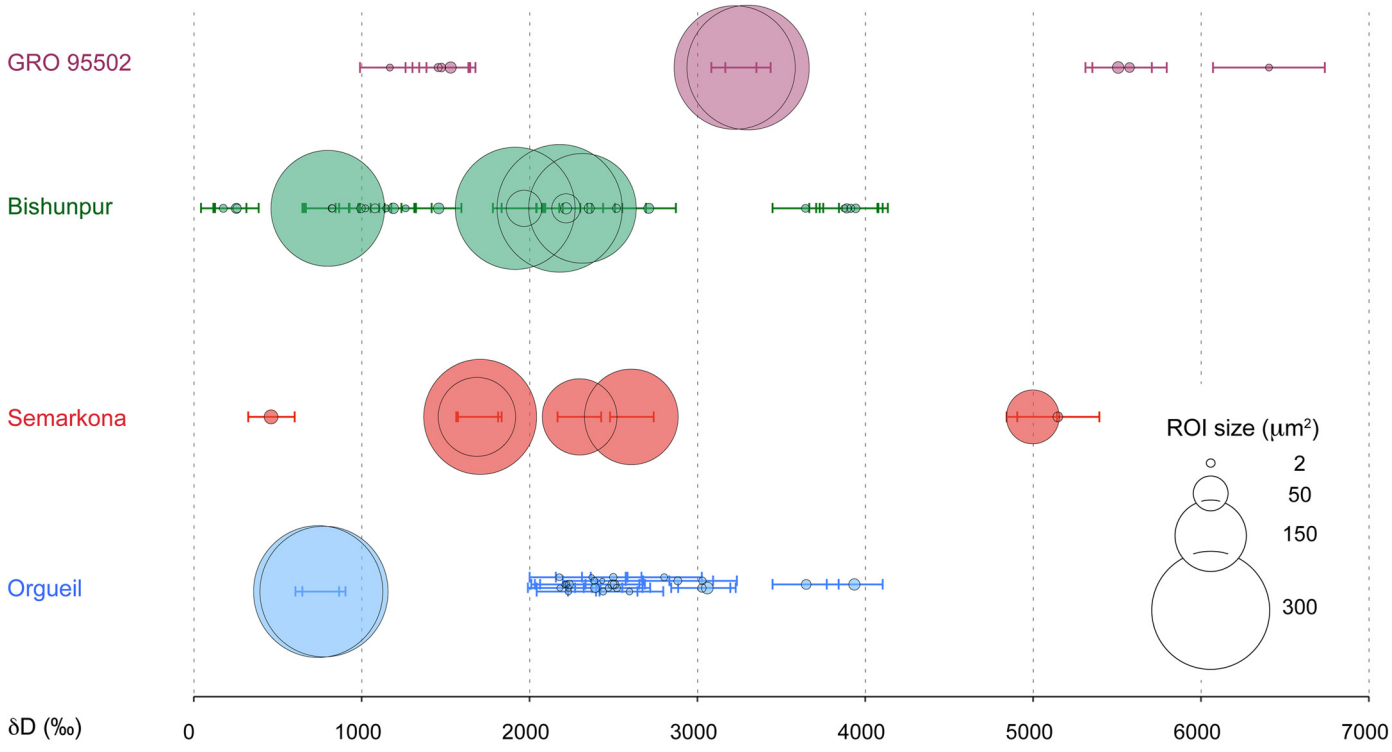

Fig. 2. δD values determined by NanoSIMS imaging, see also Table S2. See text for ROI definition. The size of the disks represents the size of each ROI. The largest circles represent the average image values. In Bishunpur IOM, some regions identified as anomalies in one image may just correspond to "normal" area in other images.

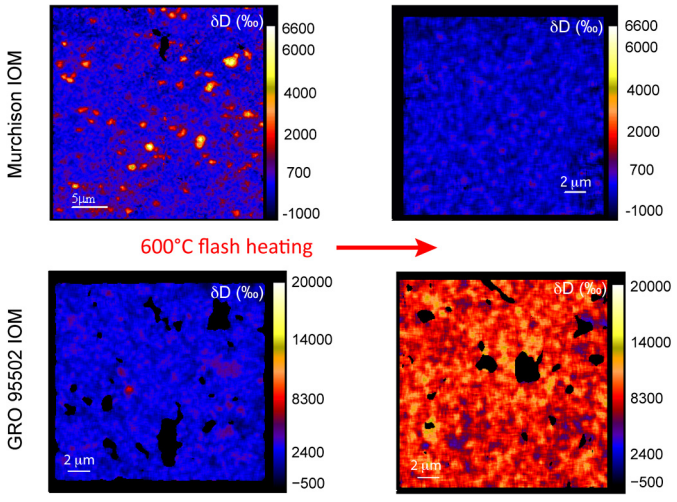

Fig. 3. Comparative evolution of δD NanoSIMS images for Murchison and GRO 95502 IOM upon 600 °C flash heating. The data for Murchison were taken from Remusat et al. (2009). In order to visualize the isotopic evolution, the color scale is the same before and after heating. The reader is advised that we have reported here, for the unheated GRO IOM on the left hand side, an image of the same areas as in Fig. 1, but the scale was modified to match the scale of the image of GRO IOM after heating (i.e. GROpyr sample), on the right hand side. For Murchison, the isotopic anomalies are destroyed and some D is lost; it results in a D-depletion. For GRO 95502, we observe an overall D-enrichment. (Colored version of this figure is available in the web version of this article.)

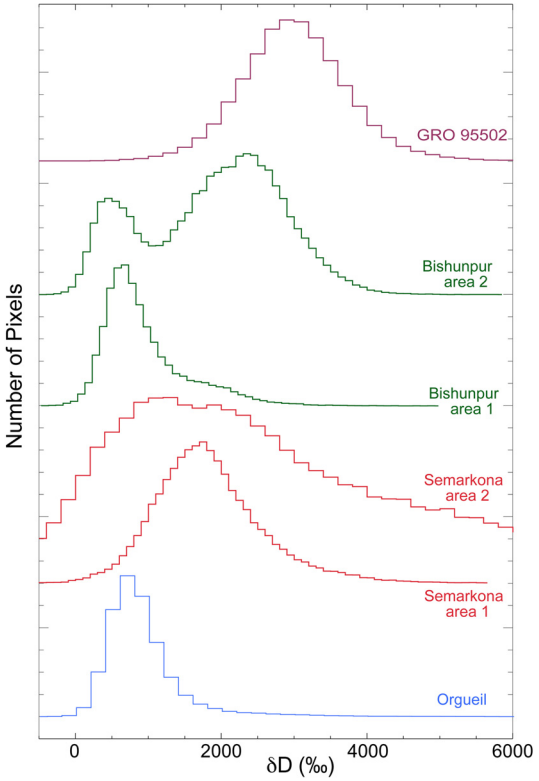

Fig. 4. Pixel (frequency) histograms (pixel value distribution) of the images reported in Fig. 1. The vertical axis is in arbitrary units and represents the number of pixels having a given δD. δD values are corrected. Bishunpur and Semarkona IOM show clearly distinct histograms.

mogeneous distribution of D and the occurrence of a single main D-rich component.

3.2. NanoSIMS imaging of N-isotopes

Semarkona, Bishunpur and GRO 95502 IOM do not display large-scale δ^{15}N heterogeneities: each investigated IOM exhibits identical mean δ^{15}N values (within error bars) over different regions (Fig. 5, Fig. 6 and Table S3). The Bishunpur IOM does not exhibit any ^{15}N anomalies, the Semarkona IOM only one (δ^{15}N > 200‰) and GRO IOM only two (δ^{15}N > 225‰). The ^{15}N anomalies

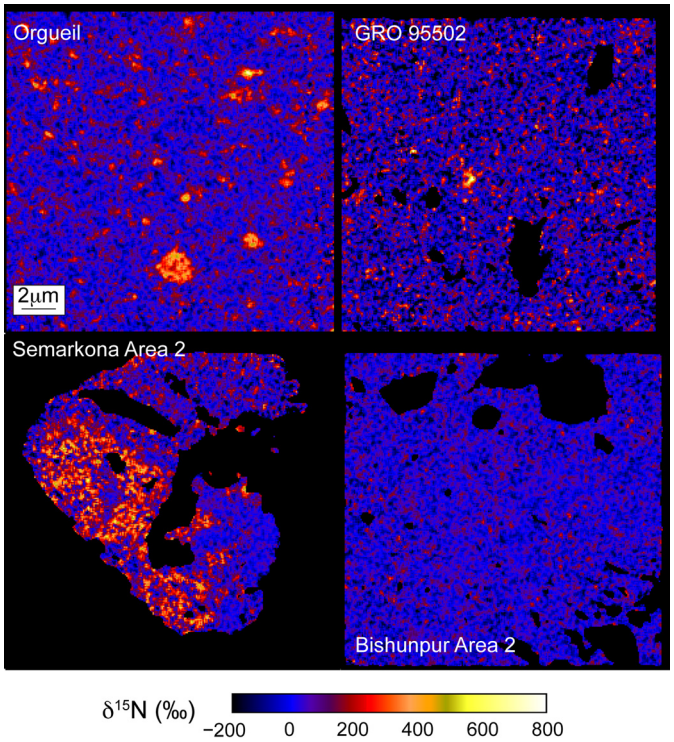

Fig. 5. NanoSIMS δ^{15}N images of the IOM of Orgueil, GRO 95502, Semarkona and Bishunpur. All the images have the same size; the color scale represents corrected δ^{15}N values. Theses images are located at the same places as the corresponding images in Fig. 1. (Colored version of this figure is available in the web version of this article.)

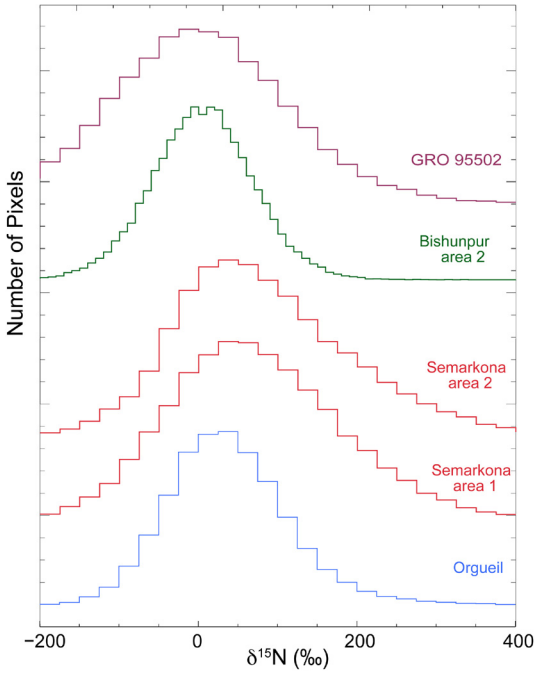

Fig. 7. Pixel (frequency) histograms (pixel value distribution) of the images reported in Fig. 5. The vertical axis is in arbitrary units and represents the number of pixels having a certain δ^{15}N. Corrected δ^{15}N are reported.

of the Semarkona and GRO 95502 IOM are spatially correlated to D anomalies (compare Figs. 1 and 5). Some of these ^{15}N anomalies exhibit significantly lower N/C values than the bulk IOM values. In contrast the Orgueil IOM exhibits numerous micron-scale ^{15}N positive ($120‰ < \delta^{15}N < 230‰$) and negative ($-200‰ < \delta^{15}N < -70‰$) anomalies; they exhibit the same N/C ratios as the bulk IOM. The occurrence of these anomalies in Orgueil IOM is consistent with data reported for different CCs (Busemann et al., 2006; Nakamura-Messenger et al., 2006; Floss and Stadermann, 2009).

While the Bishunpur IOM shows δ^{15}N histograms similar to that of Orgueil (i.e., a Gaussian curve with an FWHM of 180‰), the Semarkona and GRO 95502 IOM exhibit broader histograms with FWHM of 260‰ (Fig. 7). This may result from heterogeneities in δ^{15}N values or, more likely, from a total N abundance that is three times lower for the IOM of these chondrites compared to Bishunpur and Orgueil IOM. Such a low abundance may indeed increase

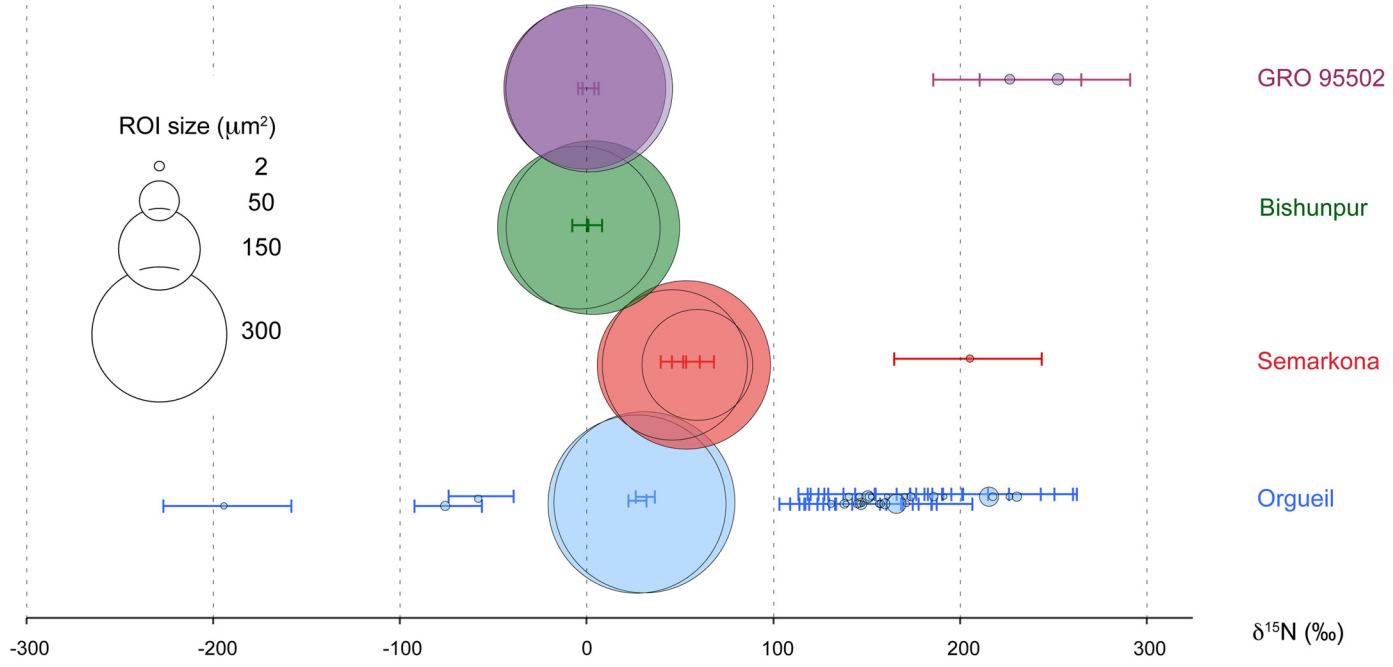

Fig. 6. δ^{15}N of isotopic anomalies detected in the IOM studied. The size of the disks represents the size of each ROI. The largest circles represent the average image values. Positive anomalies in Semarkona and GRO 95502 are rare and plot in the higher range of Orgueil IOM anomalies.

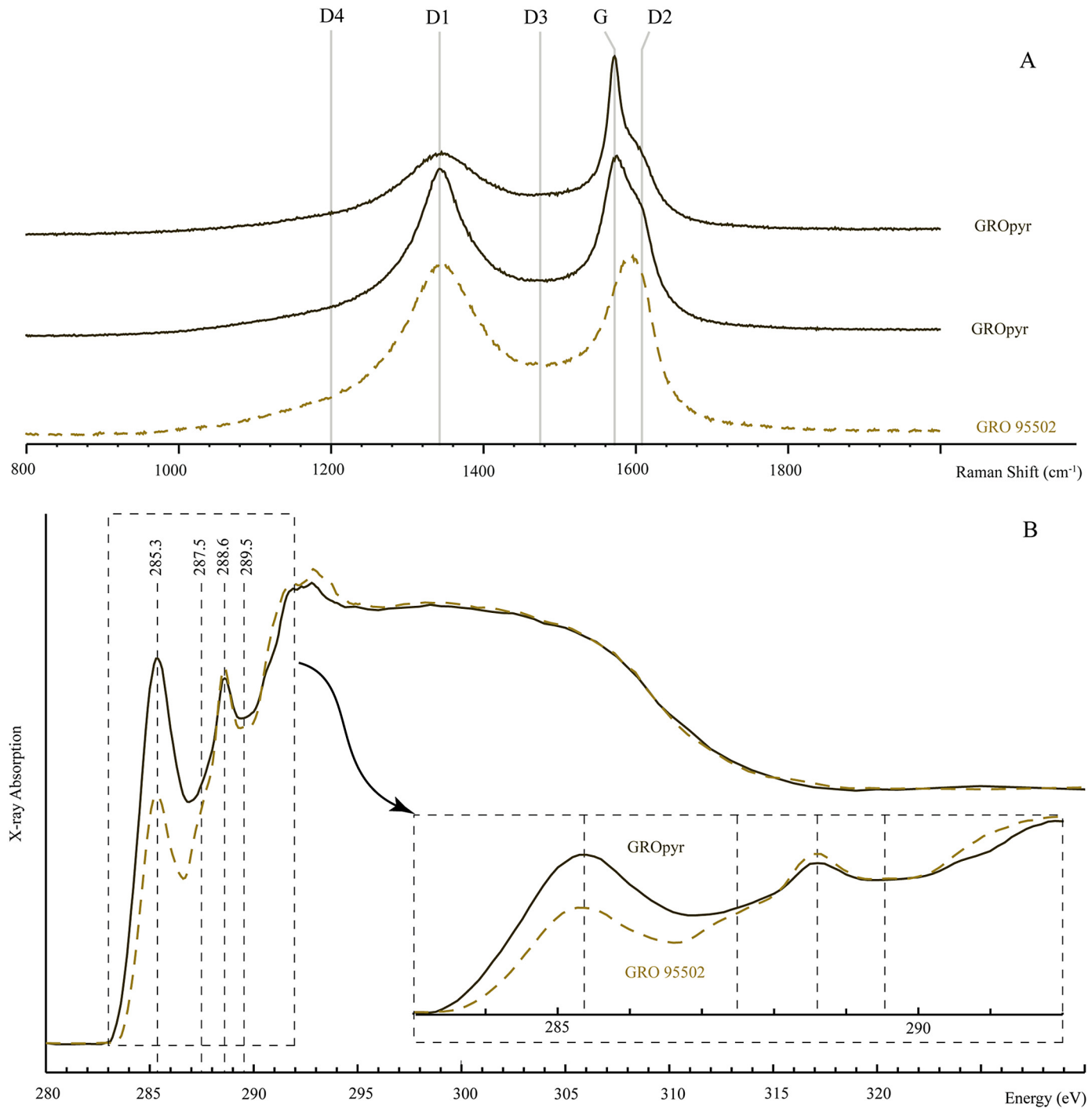

Fig. 8. Structural and molecular signature evolution of GRO IOM under thermal stress. A: Raman spectra show that GRO IOM is becoming more organized, although it gets heterogeneous. B: XANES spectra of GRO IOM and GROpyr. XANES spectra show that upon heating, GRO IOM is becoming more aromatic and is losing aliphatic C. In addition, COOH groups are less abundant.

the measurement uncertainty of each pixel and thus artificially increase the δ^{15}N variability.

3.3. Evolution of the molecular structure of GRO IOM upon heating

The molecular evolution of OC IOM was investigated by characterizing GRO IOM and GROpyr using both Raman and STXM-based XANES. The Raman signature of the GRO IOM (Fig. 8) is consistent with a moderately heated IOM, comparable to Krymka and Inman OM (Quirico et al., 2003), with two main bands of similar intensities: a quite broad D1 band at 1340 cm^{-1} and a composite G + D2 band centered at 1600 cm^{-1}. In contrast to the GRO IOM, GROpyr appears structurally heterogeneous as indicated by the two different Raman spectra that are shown in Fig. 8. Of note, all GROpyr Raman spectra exhibit a well-identified G band that dominates the signal, as well as D1 and D2 bands that vary in intensity depending on the degree of carbon organization. Overall, these Raman spectra point to thermally evolved organics having experienced partial graphitization (Bernard et al., 2010).

The XANES spectrum of GRO IOM exhibits two prominent absorption peaks at 285.3 and 288.6 eV corresponding to electronic transitions of aromatic and/or olefinic carbon (C=C) and of carbon

in carboxylic functional groups (COOH), respectively. The presence of aliphatic carbon (CH_n) can also be seen at 287.5 eV. Despite the absence of ketonic carbon (peak at 286.5 eV), this spectrum appears quite similar to that of CC IOM such as Orgueil or Murchison IOM (De Gregorio et al., 2013; Le Guillou et al., 2014). GROpyr contains significantly more aromatic/olefinic carbons than the GRO IOM together with a lower concentration of aliphatic and carboxylic carbons. The evolution of the XANES signal from GRO IOM to GROpyr is consistent with Raman data and shows molecular evolution during partial graphitization (Bernard et al., 2010).

Taken together, Raman and XANES signatures highlight the similar molecular and structural evolution undergone by both CC IOM (Bonal et al., 2007; Busemann et al., 2007; Cody and Alexander, 2005; Remusat et al., 2008) and OC IOM upon heating (flash pyrolysis at 600 °C).

4. Discussion

4.1. D and ^{15}N distributions in OC IOM

The most D-rich organic moieties in the Orgueil IOM are organic radicals (Delpoux et al., 2010), which are heterogeneously distributed in the IOM (Binet et al., 2004). The CI, CM and CR IOM have been described as assemblage of moderately D-rich organic matter associated with organic radicals extremely rich in D that constitute less than 20 vol% of the total IOM (Remusat et al., 2009). The clusters rich in organic radicals then appear as micron-size D-rich hotspots in NanoSIMS images (Remusat et al., 2009).

In contrast, very few micron-scale D anomalies have been observed in the OC IOM investigated in the present study, consistent with observations reported for the Krymka (LL 3.2) IOM (Alexander et al., 2010). Nevertheless, the D distribution in OC IOM is not homogeneous. Semarkona and Bishunpur IOM seem to be constituted by at least two components that can be resolved at the scale of several microns (Figs. 1 and 4). These organic components may have experienced different conditions on the parent body (Alexander et al., 2010) or may have originally been different, i.e. they may have had distinct δD signatures before being accreted. It has been shown that large variations of clay mineral isotope signatures and heterogeneities of organic isotopic signatures are not correlated within the matrix of Semarkona (Piani et al., 2015). This observation strengthens the scenario of the accretion of distinct organic precursors having different isotopic signatures.

The occurrence of large domains with distinct D/H is intriguing. Analytical bias during NanoSIMS imaging can be ruled out as such distribution is not observed in terrestrial standards or Orgueil IOM measured under the same experimental conditions. In addition, the average values obtained for Semarkona and Bishunpur IOM are consistent with previous measurements (Alexander et al., 2007), thereby disproving the possibility of an HF/HCl dissolution artifact (it is unlikely that HF/HCl treatments would induce such D-transfer between organic moieties). The occurrence of these large domains with distinct D/H may result from the intrinsic nature of the different components of the IOM. OCs exhibit micrometric organic grains together with a diffuse organic component within the matrix, as observed in CCs (Le Guillou et al., 2014; Piani et al., 2015). During HF/HCl dissolution, organic components with similar affinities may gather together forming 10–20 µm large aggregates that may escape destruction during the centrifugation and drying steps.

Despite variable high D/H values, the OC IOM investigated present an almost homogeneous N-isotope composition close to $\delta^{15}N = 0‰$. Alexander et al. (2007, 2010) reported very large D-enrichment in bulk IOM from various OCs, associated with Earth-like N isotopic compositions using conventional isotope ratio mass spectrometry. This is in contrast to the CCs where the D-richest IOM also exhibit large ^{15}N-enrichments. Again, such differences may not be explained by different parent body evolution but rather by the accretion of both D- and ^{15}N-rich organics in CRs and a few CMs while only D-rich organics were accreted in OCs. The very few ^{15}N anomalies in OC IOM exhibit large D-enrichments (making them both D- and ^{15}N-rich hotspots). Ion–molecule or grain surface chemistry in cold environments could explain both D- and ^{15}N-enrichments, their scarcity possibly resulting from their sensitivity to the thermal metamorphism that occurred on OC parent bodies.

4.2. Thermal evolution of OC IOM

While the bulk δ^{15}N signatures do not appear to be sensitive to temperature conditions, the present investigations of three UOCs of increasing metamorphic grades (Semarkona (LL3.0), Bishunpur (LL3.15) and GRO 95502 (L3.2)) demonstrate an increase of δD values with increasing metamorphism. In contrast, the D/H and H/C ratios of CC IOM decrease with increasing metamorphism (Alexander et al., 2007). In other words, OC and CC IOM exhibit opposite trends in the D/H vs. H/C plot (Alexander et al., 2010), even though the structural evolution of OC and CC IOM are similar with increasing temperature (Quirico et al., 2003; Bonal et al., 2007).

Thermal degradation experiments (flash heating) performed on Murchison IOM demonstrated that D-rich hotspots do not sustain temperature (Remusat et al., 2009). Such result makes sense if hotspots concentrate D-rich organic radicals that can be easily thermally destabilized (Remusat et al., 2009). Furthermore, the IOM of the Kainsaz chondrite (CO3.6), which lacks D-rich hotspots, contains a very low amount of radicals (Remusat et al., 2008, 2009). In contrast, the present study demonstrates that the D/H ratio of GRO IOM increases with increasing temperature (GROpyr D/H is twice as large as GRO IOM) despite a structural and molecular evolution similar to that of CC IOM. Of the two organic components described in Section 4.1, one is likely thermally recalcitrant (the D-rich one) while the second evolves into graphitized material through H loss (its H/C decreases with increasing temperature). Indeed, as indicated by Raman and STXM-based XANES spectroscopy, the GRO IOM undergoes a structural reorganization concomitant with an increase of its aromatic/aliphatic carbon ratio as temperature increases. This evolution, typical of the carbonization process (Bernard et al., 2010), is also observed for CC IOM affected by thermal metamorphism (Quirico et al., 2003; Bonal et al., 2007; Busemann et al., 2007; Remusat et al., 2008).

The present contribution thus demonstrates that the organic D-rich reservoirs in OC and CC IOM are different. While CC IOM loses its most D-rich organic reservoir upon heating, OC IOM loses its D-poor organic H reservoir. This is consistent with the evolution from a bimodal D/H histogram, as seen in the Semarkona and Bishunpur IOM, to a more homogeneous distribution in the IOM of the more heated GRO 95502 (Fig. 4). This is also consistent with NanoSIMS data reported for the IOM of the Krymka 3.2 OC (Alexander et al., 2010).

In summary, in contrast to that of CC IOM, the D-rich component of OC IOM is not borne by organic radicals but rather by thermally recalcitrant organic moieties. This recalcitrance would explain the evolution reported by Alexander et al. (2007, 2010) for bulk OC IOM in the D/H vs. H/C plot, i.e. the increase of the D/H ratio of OC IOM may directly result from an increase of metamorphic temperature experienced by OC parent bodies.

4.3. Origin of the D-rich organic reservoir in OCs

Alexander et al. (2010) suggested that the D-rich component of UOC IOM results from isotopic exchange between IOM and D-rich

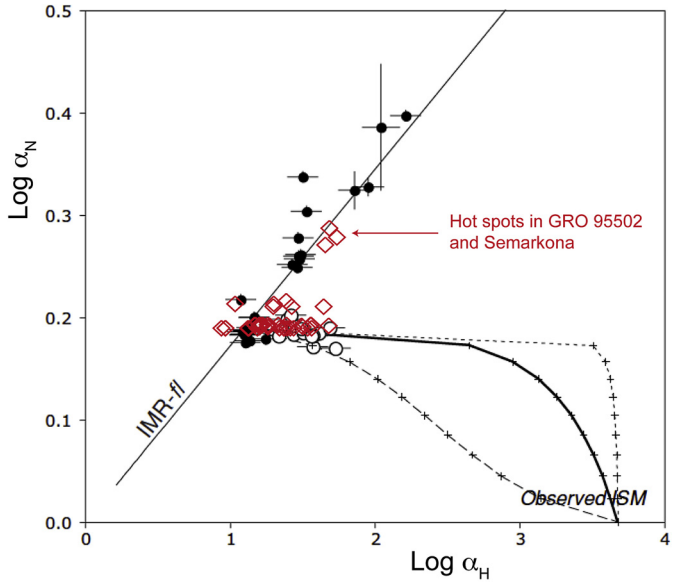

Fig. 9. Comparison of the isotopic composition of OC IOM (this study) with the model by Aléon (2010). The N isotopic fractionation between organics and the protosolar gas is reported versus the H isotopic fractionation. Black dots represent sample of group 1 as defined by Aléon: IOM in CC and their hotspots, values taken from the literature until 2010. In open black dots are reported bulk IOM of unequilibrated OC (Alexander et al., 2007). Curves describe mixing between observed interstellar molecules (*Observed ISM*) and typical CM chondrite IOM with: isochemical mixing (plain curve), mixing with Murchison CHON and ISM HCN (dashed curves) and with Murchison HCN and ISM CHON (dotted curve). ISM values are taken from Millar et al. (1989), Turner (2001) and Roueff et al. (2007). Details and references can be found in Aléon (2010). Our data for OC IOM are reported as red open diamonds. It must be noted that three hotspots observed in Semarkona and GRO 95502 fit with the ion/molecule reaction fractionation line (IMR-fl) defined by Aléon (2010).

water, such as the water reported in UOCs by Deloule and Robert (1995). This water would have been enriched in D through distillation process resulting from the progressive reduction of water by reaction with Fe. Yet, Piani et al. (2015) recently reported the absence of spatial correlation between IOM and water D/H ratios as well as huge heterogeneities in the δD values of Semarkona phyllosilicates (up to $\delta D = 10{,}000‰$) that may not result from distillation processes. Aléon (2010) suggested an alternative hypothesis: he interpreted the D-enrichment of OC IOM as resulting from the presence of presolar organics synthesized in the interstellar medium (ISM). In this model, the D/H ratio of OC IOM results from mixing between IOM similar to that of Murchison and extremely D-rich ISM organics (1 at% at most), with no significant ^{15}N-enrichment relative to solar system organic matter. Hence, according to Aléon (2010) and Piani et al. (2015), both D-rich organics and D-rich water ice from primitive reservoir(s) would have been accreted and preserved within OC parent-bodies.

In Fig. 9, the data collected in the present study are compared to previous measurements of CC and OC IOM, IDPs and Hale–Bopp HCN as well as models showing fractionation due to ion–molecule reactions (IMR-fl) and mixing between a component akin to CM chondrites IOM (Murchison) and observed molecules in the interstellar medium (Aléon, 2010 and references therein). H and N isotopic compositions are expressed as isotopic fractionation factors (αH and αN) between organic matter and the protosolar gas, the composition of which is $D/H = 21 \times 10^{-6}$ (Geiss and Reeves, 1981) and $^{15}N/^{14}N = 2.36 \times 10^{-3}$ (Meibom et al., 2007). The Genesis mission since reported that protosolar $^{15}N/^{14}N = 2.27(\pm 0.03) \times 10^{-3}$ (Marty et al., 2011).

The present data are consistent with previous OC IOM data and fall on the mixing curve proposed by Aléon (2010). Most of the D-enrichments reported here are not associated with any significant enrichment in ^{15}N. At the micro-scale, no D anomalies correspond to the ISM organic component with D/H = 0.1 predicted by Aléon (2010). Thus, if mixing has occurred, it has to be at a very fine scale, below a few tens of nanometers, i.e. at the molecular scale. Hence, OC IOM contains interstellar molecular moieties or was formed from ISM precursors that were incorporated into the OC IOM during solar system formation. Of note, D and ^{15}N anomalies of OC IOM follow the trend defined by the simultaneous H and N isotopic fractionation by ion/molecule reactions occurring in the protosolar nebula or in the parent molecular cloud (IMR-fl, Fig. 9); hence, they may have formed in the solar system nebula by ion/molecule reactions (Aléon, 2010).

5. Conclusion

The present study shows that the D and ^{15}N distributions in CC and OC IOM are different. The OC IOM does not exhibit numerous micron-scale isotopic anomalies (both D- and ^{15}N-rich), even in the least metamorphosed, Semarkona. In addition, OC IOM appears to be composed of two main isotopic reservoirs, the D-richer being thermally recalcitrant. Thermal degradation experiments (flash heating) indeed demonstrate that the D/H ratio of OC IOM increases with increasing temperature despite a structural and molecular evolution similar to that of CC IOM as indicated by Raman and STXM-based XANES spectroscopy. Based on these observations, we suggest that CCs and OCs did not accrete the same organic precursors, as a consequence of spatial and/or temporal heterogeneities in the solar nebula. This indicates that the organic content of the protosolar nebula was probably evolving during parent body formation. The common organic precursor concept should be revised, as CC, OC, and enstatite chondrites appear to contain IOM with different properties (Alexander et al., 2007; Piani et al., 2012b). We suggest that the D-rich, thermally recalcitrant component of OC IOM may have formed in the ISM, thus supporting the vision of Aléon (2010) stating that OC IOM is "polluted" by minute amount of ISM organics.

Acknowledgements

We are grateful to M. Garcia (curator of the Caltech GPS sample collection) for having kept the precious IOM of Semarkona and Bishunpur prepared 30 years ago. We thank Aurélien Thomen and François Robert for helpful discussion and Roger Hewins for his comments on the manuscript. The National NanoSIMS Facility at the Museum National d'Histoire Naturelle was established by funds from the CNRS, Région Île de France, Ministère délégué à l'Enseignement supérieur et à la Recherche, and the Muséum itself. STXM data were acquired at beamline 5.3.2.2 at the ALS, which is supported by the Director of the Office of Science, Department of Energy, under Contract No. DE-AC02-05CH11231. Special thanks go to David Kilcoyne for his expert support of the 5.3.2.2 STXM at the ALS. L.R. thanks the Programme National de Planétologie (PNP) of CNRS/INSU for financial support. We thank Hikaru Yabuta, Conel Alexander and Editor Bernard Marty for their comments that helped to improve the quality of the paper.

Appendix A. Supplementary material

Supplementary material related to this article can be found online at http://dx.doi.org/10.1016/j.epsl.2015.12.009.

References

Aléon, J., 2010. Multiple origins of nitrogen isotopic anomalies in meteorites and comets. Astrophys. J. 722, 1342.

Alexander, C.M.O'D., Barber, D.J., Hutchison, R., 1989. The microstructure of Semarkona and Bishunpur. Geochim. Cosmochim. Acta 53, 3045–3057.

Alexander, C.M.O'D., Fogel, M., Yabuta, H., Cody, G.D., 2007. The origin and evolution of chondrites recorded in the elemental and isotopic compositions of their macromolecular organic matter. Geochim. Cosmochim. Acta 71, 4380–4403.

Alexander, C.M.O'D., Newsome, S.D., Fogel, M.L., Nittler, L.R., Busemann, H., Cody, G.D., 2010. Deuterium enrichments in chondritic macromolecular material—implications for the origin and evolution of organics, water and asteroids. Geochim. Cosmochim. Acta 74, 4417–4437.

Alleon, J., Bernard, S., Remusat, L., Robert, F., 2015. Estimation of nitrogen-to-carbon ratios of organics and carbon materials at the submicrometer scale. Carbon 84, 290–298.

Bernard, S., Beyssac, O., Benzerara, K., 2008. Raman mapping using advanced line-scanning systems: geological applications. Appl. Spectrosc. 62, 1180–1188.

Bernard, S., Beyssac, O., Benzerara, K., Findling, N., Tzvetkov, G., Brown Jr., G.E., 2010. XANES, Raman and XRD study of anthracene-based cokes and saccharose-based chars submitted to high-temperature pyrolysis. Carbon 48, 2506–2516.

Beyssac, O., Brunet, F., Petitet, J.-P., Goffé, B., Rouzaud, J.-N., 2003. Experimental study of the microtextural and structural transformations of carbonaceous materials under pressure and temperature. Eur. J. Mineral. 15, 937–951.

Binet, L., Gourier, D., Derenne, S., Robert, F., 2002. Heterogeneous distribution of paramagnetic radicals in insoluble organic matter from the Orgueil and Murchison meteorites. Geochim. Cosmochim. Acta 66, 4177–4186.

Binet, L., Gourier, D., Derenne, S., Robert, F., Ciofini, I., 2004. Occurrence of abundant diradicaloid moieties in the insoluble organic matter from the Orgueil and Murchison meteorites: a fingerprint of its extraterrestrial origin? Geochim. Cosmochim. Acta 68, 881–891.

Bonal, L., Bourot-Denise, M., Quirico, E., Montagnac, G., Lewin, E., 2007. Organic matter and metamorphic history of CO chondrites. Geochim. Cosmochim. Acta 71, 1605–1623.

Busemann, H., Alexander, C.M.O'D., Nittler, L.R., 2007. Characterization of insoluble organic matter in primitive meteorites by microRaman spectroscopy. Meteorit. Planet. Sci. 42, 1387–1416.

Busemann, H., Young, A.F., Alexander, C.M.O'D., Hoppe, P., Mukhopadhyay, S., Nittler, L.R., 2006. Interstellar chemistry recorded in organic matter from primitive meteorites. Science 312, 727–730.

Cody, G.D., Alexander, C.M.O'D., 2005. NMR studies of chemical and structural variation of insoluble organic matter from different carbonaceous chondrite groups. Geochim. Cosmochim. Acta 69, 1085–1097.

De Gregorio, B.T., Stroud, R.M., Nittler, L.R., Alexander, C.M.O'D., et al., 2013. Isotopic and chemical variation of organic nanoglobules in primitive meteorites. Meteorit. Planet. Sci. 48, 904–928.

Deloule, E., Robert, F., 1995. Interstellar water in meteorites? Geochim. Cosmochim. Acta 59, 4695–4706.

Delpoux, O., Gourier, D., Vezin, H., Binet, L., Derenne, S., Robert, F., 2010. Biradical character of D-rich carriers in the insoluble organic matter of carbonaceous chondrites: a relic of the protoplanetary disk chemistry. Geochim. Cosmochim. Acta 75, 326–336.

Floss, C., Stadermann, F.J., 2009. High abundances of circumstellar and interstellar C-anomalous phases in the primitive CR3 chondrites QUE 99177 and MET 00426. Astrophys. J. 697, 1242–1255.

Geiss, J., Reeves, H., 1981. Deuterium in the solar system. Astron. Astrophys. 93, 189–199.

Hayatsu, R., Winans, R.E., Scott, R.G., McBeth, R.L., Moore, L.P., Studier, M.H., 1980. Phenolic ethers in the organic polymer of the Murchison meteorite. Science 207, 1202–1204.

Hitchcock, A.P., Dynes, J.J., Johansson, G., Wang, J., Botton, G., 2008. Comparison of NEXAFS microscopy and TEM-EELS for studies of soft matter. Micron 39, 311–319.

Kilcoyne, A.L.D., Tyliszczak, T., Steele, W.F., Fakra, S., et al., 2003. Interferometer-controlled scanning transmission X-ray microscopes at the Advanced Light Source. J. Synchrotron Radiat. 10, 125–136.

Le Guillou, C., Bernard, S., Brearley, A.J., Remusat, L., 2014. Evolution of organic matter in Orgueil, Murchison and Renazzo during parent body aqueous alteration: in situ investigations. Geochim. Cosmochim. Acta 131, 368–392.

Marty, B., Chaussidon, M., Wiens, R.C., Jurewicz, A.J.G., Burnett, D.S., 2011. A ^{15}N-poor isotopic composition for the Solar System as shown by Genesis solar wind samples. Science 332, 1533–1536.

Meibom, A., Krot, A.N., Robert, F., Mostefaoui, S., Russell, S.S., Petaev, M.I., Gounelle, M., 2007. Nitrogen and carbon isotopic composition of the Sun inferred from a high-temperature solar nebular condensate. Astrophys. J. 656, L33–L36.

Millar, T.J., Bennett, A., Herbst, E., 1989. Deuterium fractionation in dense interstellar clouds. Astrophys. J. 340, 906–920.

Nakamura-Messenger, K., Messenger, S., Keller, L.P., Clemett, S.J., Zolensky, M.E., 2006. Organic globules in the Tagish Lake meteorite: remnants of the protosolar disk. Science 314, 1439–1442.

Orthous-Daunay, F.R., Quirico, E., Lemelle, L., Beck, P., deAndrade, V., Simionovici, A., Derenne, S., 2010. Speciation of sulfur in the insoluble organic matter from carbonaceous chondrites by XANES spectroscopy. Earth Planet. Sci. Lett. 300, 321–328.

Piani, L., Remusat, L., Robert, F., 2012a. Determination of the H isotopic composition of individual components in fine-scale mixtures of organic matter and phyllosilicates with the nanoscale secondary ion mass spectrometry. Anal. Chem. 84, 10199–10206.

Piani, L., Robert, F., Beyssac, O., Binet, L., Bourot-Denise, M., Derenne, S., Le Guillou, C., Marrocchi, Y., Mostefaoui, S., Rouzaud, J.-N., Thomen, A., 2012b. Structure, composition, and location of organic matter in the enstatite chondrite Sahara 97096 (EH3). Meteorit. Planet. Sci. 47, 8–29.

Piani, L., Robert, F., Remusat, L., 2015. Micron-scale D/H heterogeneity in chondrite matrices: a signature of the pristine solar system water? Earth Planet. Sci. Lett. 415, 154–164.

Quirico, E., Raynal, P.I., Bourot-Denise, M., 2003. Metamorphic grade of organic matter in six unequilibrated ordinary chondrites. Meteorit. Planet. Sci. 38, 795–811.

Ravel, B., Newville, M., 2005. ATHENA, ARTEMIS, HEPHAESTUS: data analysis for X-ray absorption spectroscopy using IFEFFIT. J. Synchrotron Radiat. 12, 537–541.

Remusat, L., 2015. Organics in primitive meteorites. In: Lee, M.R., Leroux, H. (Eds.), Planetary Mineralogy. In: EMU Notes in Mineralogy, vol. 15. The European Mineralogical Union, ISBN 978-0903056-55-7, pp. 33–65 (Chapter 2).

Remusat, L., Derenne, S., Robert, F., Knicker, H., 2005. New pyrolytic and spectroscopic data on Orgueil and Murchison insoluble organic matter: a different origin than soluble? Geochim. Cosmochim. Acta 69, 3919–3932.

Remusat, L., Le Guillou, C., Rouzaud, J.-N., Binet, L., Robert, F., Derenne, S., 2008. Molecular study of the insoluble organic matter of Kainsaz CO_3 carbonaceous chondrite: comparison with CI and CM IOM. Meteorit. Planet. Sci. 43, 1099–1111.

Remusat, L., Robert, F., Meibom, A., Mostefaoui, S., et al., 2009. Proto-planetary disk chemistry recorded by D-rich organic radicals in carbonaceous chondrites. Astrophys. J. 698, 2087–2092.

Robert, F., Epstein, S., 1982. The concentration and isotopic composition of hydrogen, carbon and nitrogen in carbonaceous meteorites. Geochim. Cosmochim. Acta 46, 81–95.

Roueff, E., Herbst, E., Lis, D.C., Phillips, T.G., 2007. The effect of an increased elemental D/H ratio on deuterium fractionation in the cold interstellar medium. Astrophys. J. 661, L159–L162.

Sears, D.W.G., Morse, A.D., Hutchison, R., Guimon, R.K., et al., 1995. Metamorphism and aqueous alteration in low petrographic type ordinary chondrites. Meteoritics 30, 169.

Solomon, D., Lehmann, J., Kinyangi, J., Liang, B., et al., 2009. Carbon (1s) NEXAFS spectroscopy of biogeochemically relevant reference organic compounds. Soil Sci. Soc. Am. J. 73, 1817–1830.

Thomen, A., Robert, F., Remusat, L., 2014. Determination of the nitrogen abundance in organic materials by NanoSIMS quantitative imaging. J. Anal. At. Spectrom. 29, 512–519.

Turner, B.E., 2001. Deuterated molecules in translucent and dark clouds. Astron. Astrophys. Suppl. Ser. 136, 579–629.

Wang, J., Morin, C., Li, L., Hitchcock, A.P., Scholl, A., Doran, A., 2009. Radiation damage in soft X-ray microscopy. J. Electron Spectrosc. Relat. Phenom. 170, 25–36.

Weisberg, M.K., McCoy, T.J., Krot, A.N., 2006. Systematics and evaluation of meteorite classification. In: Lauretta, D., McSween, H.Y.J.J. (Eds.), Meteorites and the Early Solar System II. University of Arizona Press, Tucson, USA, pp. 19–52.

Yang, J., Epstein, S., 1983. Interstellar organic matter in meteorites. Geochim. Cosmochim. Acta 47, 2199–2216.

Zanda, B., Bourot-Denise, M., Hewins, R.H., 1995. Condensate sulfide and its metamorphic transformations in primitive chondrites. Meteoritics 30, 605.